Princeton Plasma Physics Laboratory

PPPL- 4791

PPPL- 4791

A New Scheme for Stigmatic X-ray Imaging with Large Magnification

M. Bitter, K.W. Hill, L.F. Delgado-Aprico, N.A. Pablant, S. Scott, F. Jones, P. Beiersdorfer, E. Wang, M. Sanchez del Rio, T.A. Caughey and J. Brunner

August, 2012

Prepared for the U.S. Department of Energy under Contract DE-AC02-09CH11466.

Princeton Plasma Physics Laboratory
Report Disclaimers

Full Legal Disclaimer

Trademark Disclaimer

PPPL Report Availability

Princeton Plasma Physics Laboratory:

http://www.pppl.gov/techreports.cfm

Office of Scientific and Technical Information (OSTI):

http://www.osti.gov/bridge

Related Links:

U.S. Department of Energy

Office of Scientific and Technical Information

Fusion Links

A new scheme for stigmatic x-ray imaging with large magnification[a)]

M. Bitter,[1,b)] K. W. Hill,[1] L. F. Delgado-Aparicio,[1] N. A. Pablant,[1] S. Scott,[1] F. Jones,[1] P. Beiersdorfer,[2] E. Wang,[2] M. Sanchez del Rio,[3] T. A. Caughey,[4] and J. Brunner[4]
[1]*Princeton Plasma Physics Laboratory, Princeton, New Jersey 08543, USA*
[2]*Physics Division, Lawrence Livermore National Laboratory, Livermore, California 94550, USA*
[3]*European Synchrotron Radiation Facility, BP 220, 38043-Grenoble Cedex, France*
[4]*Inrad Optics, 181 Legrand Avenue, Northvale, New Jersey 07647, USA*

(Presented 7 May 2012; received 7 May 2012; accepted 7 July 2012; published online 3 August 2012)

This paper describes a new x-ray scheme for stigmatic imaging. The scheme consists of one convex spherically bent crystal and one concave spherically bent crystal. The radii of curvature and Bragg reflecting lattice planes of the two crystals are properly matched to eliminate the astigmatism, so that the conditions for stigmatic imaging are met for a particular wavelength. The magnification is adjustable and solely a function of the two Bragg angles or angles of incidence. Although the choice of Bragg angles is constrained by the availability of crystals, this is not a severe limitation for the imaging of plasmas, since a particular wavelength can be selected from the bremsstrahlung continuum. The working principle of this imaging scheme has been verified with visible light. Further tests with x rays are planned for the near future. © *2012 American Institute of Physics*. [http://dx.doi.org/10.1063/1.4739069]

I. INTRODUCTION

X-ray pinhole cameras are being used for imaging small laser produced plasmas.[1,2] These cameras are capable of providing images with large magnification. However, the disadvantages are that the diameter of the pinhole must be small, of the order of 4–50 μm, to obtain high spatial resolution and that—in order to obtain sufficient photon throughput—the pinhole must be placed close to the x-ray source, where it is at risk of being destroyed during an experiment.

These shortcomings of x-ray pinhole cameras can be overcome by using the focusing properties of spherically bent crystals to form an image of the x-ray source. The photon throughput can thereby be increased by several orders of magnitude since, instead of a pinhole, the much larger area of a crystal serves as an entrance aperture. The crystal can also be placed at a larger distance from the source than a pinhole. A major problem for imaging with spherically bent crystals are, however, the astigmatic image distortions, which occur for a non-normal incidence of x rays on the crystal. To avoid this problem, the imaging schemes which make use of the focusing properties of only one spherically bent crystal must be operated at Bragg angles near 90°—regardless of whether the image is formed by the directly emitted radiation[1] or backlighting of the object with an external x-ray source.[3] The detector must then be placed near the x-ray source, where it is at risk of being damaged by debris ejected from the x-ray source. Another disadvantage of this "near normal incidence constraint" is that the number of suitable wavelengths is restricted by the availability of crystals with appropriate 2d-spacings for Bragg angles near 90°—see Table 2 in Ref. 1.

As an example, we mention the recent imaging scheme of Loupias *et al.*,[4] a backlighting system with a Bragg angle of 76.7°, where the object and x-ray source were placed inside the Rowland circle of a spherically bent crystal, at positions, which were carefully chosen by ray-tracing calculations. Although these authors obtained spatial resolutions of <10 μm in the *meridional* plane and 25 μm in the *sagittal* plane that were adequate for their experiments, the fact that the spatial resolutions in those two planes were different is indicative of astigmatic image distortions.

The astigmatism of spherically bent crystals or spherical mirrors results from the fact that the imaging equations for rays in the plane of dispersion (*meridional rays*) and rays in a plane perpendicular to the dispersion plane (*sagittal rays*) are different:

$$\frac{1}{p}+\frac{1}{q}=\frac{2}{R\bullet\sin(\theta)} \qquad (for\ meridional\ rays) \qquad (1)$$

and

$$\frac{1}{p}+\frac{1}{q}=\frac{2\bullet\sin(\theta)}{R} \qquad (for\ sagittal\ rays). \qquad (2)$$

Here, p and q are the distances of object and image from the center of the crystal, and R and θ are the radius of curvature of the crystal and the Bragg angle, respectively. Equations (1) and (2) are also known as Coddington's equations.[5] It is clear from these equations that stigmatic imaging with a spherically bent crystal is only possible for the Bragg angle $\theta = 90°$. To enable stigmatic imaging for Bragg angles different from 90°, toroidally bent crystals have been used[6] or proposed,[7] where the ratio of the radii of curvature in the *sagittal* and *meridional* planes was $R_s/R_m = \sin^2(\theta)$. In this way, it is possible to obtain stigmatic imaging for one particular Bragg angle θ. It was, however, pointed out by Podorov,

[a)]Contributed paper, published as part of the Proceedings of the 19th Topical Conference on High-Temperature Plasma Diagnostics, Monterey, California, May 2012.
[b)]Author to whom correspondence should be addressed. Electronic mail: bitter@pppl.gov.

Nazarkin, and Förster[8] that "as a rule the x-ray images obtained with one toroidally bent crystal have different sorts of aberrations"; and to minimize those aberrations these authors proposed an "optimized two-crystal arrangement," consisting of two toroidally bent crystals, where one crystal had a concave and the other a convex curvature.[8] It is also noteworthy that the Bragg angle for the schemes discussed in Ref. 8 was $\theta = 83^\circ$, i.e., still close to 90°.

We have recently proposed different types of imaging schemes,[9–11] where the astigmatism can be fully eliminated by the use of two spherically bent crystals (or reflectors), so that stigmatic imaging is possible for almost arbitrary Bragg angles or angles of incidence. In this paper, we describe a new scheme which is related to these earlier schemes and which can provide images with a large magnification.

II. WORKING PRINCIPLE AND TESTS

A. Working principle

This new x-ray imaging scheme is shown in Fig. 1. It consists of one convex spherically bent crystal, C1, and one concave spherically bent crystal, C2, and by satisfying the following conditions, it is optimized for a particular wavelength, λ: **(a)** The two crystal spheres are concentric about a point M, see Fig. 1. The ray pattern is, therefore, symmetric with respect to rotations about any axis through M. **(b)** The radii of curvature, R_1 and R_2, of the two crystal spheres and the 2d-spacings of the Bragg reflecting crystal lattice planes are properly matched, such that $R_1 \cos(\Theta_1) = R_2 \cos(\Theta_2) = RT$, where Θ_1 and Θ_2 are the Bragg angles for rays of the wavelength, λ, on crystal-1 and crystal-2, respectively. These rays must also be tangential to the concentric circles with radii $R_1 \cos(\Theta_1)$ and $R_2 \cos(\Theta_2)$ about M. Because of condition (b) these two circles are identical. The Johann focusing errors[12] of the two crystals are, therefore, also identical and overlap exactly, such that the Bragg condition is simultaneously fulfilled at all points on the two crystal surfaces. **(c)** The Bragg angles, Θ_1 and Θ_2, for the convex crystal and concave crystal are $<45^\circ$ and $>45^\circ$, respectively. This condition assures that the two crystals and the image, at point N, are on the same side of the object, which is at point O. An implementation of this imaging scheme at an experiment is thereby facilitated.

To explain the working principle, we assume at first that both crystals are concave spherically bent crystals and discuss the images, which each crystal would independently produce of a source at P, see Fig. 1. Here, P is the point of intersection of the Rowland circles for the two crystals. This point is also on the circle with the radius RT about M. The distances from P to the points, C1 and C2, the central points on the two crystal surfaces, are therefore equal to $R_1 \sin(\Theta_1)$ and $R_2 \sin(\Theta_2)$, respectively. The source dimensions are assumed to be at least of the size of the Johann error,[12] so that the source can supply rays of the wavelength, λ, for Bragg reflection at any point on the two crystal surfaces. Inserting $p = R_{1,2} \sin(\Theta_{1,2})$ in Eqs. (1) and (2) and solving for q, one obtains $q_{1,2}^{(m)} = R_{1,2} \sin(\theta_{1,2})$ and $q_{1,2}^{(s)} = -R_{1,2} \sin(\theta_{1,2}) / \cos(2\theta_{1,2})$; these are the distances of the *meridional* images, at P1 and P2, and the *sagittal* images, at O and N, from C1 and C2, respectively. Here, $q_2^s > 0$, since $\Theta_2 > 45^\circ$, and $q_1^s < 0$, since

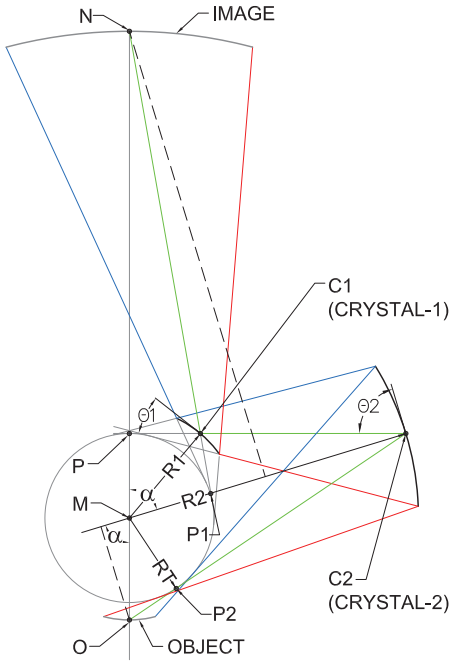

FIG. 1. Stigmatic imaging scheme as described in the text for Bragg angles $\Theta_1 = 40^\circ$ and $\Theta_2 = 73^\circ$.

$\Theta_1 < 45^\circ$. The *sagittal* image produced by crystal-2 of a small, approximate point source at P is a *real* image (actually a line image) at the point O in front of crystal-2. By contrast, the *sagittal* image produced by crystal-1 is a *virtual* line image, located at N in the dispersive plane behind crystal-1. This means that the *sagittal* rays, after Bragg reflection from crystal-1, are divergent, so that they seem to emanate from a *virtual* line source at N behind crystal-1. If we now replace the *virtual* line source at N by a *real* line source and assume that crystal-1 is a convex spherically bent crystal, we see that the *sagittal* and *meridional* rays, which emanate from this line source at N, are divergent after Bragg reflection from crystal-1 and appear to come from a *virtual* "point" source at P. With respect to crystal-2, the ray pattern is the same as before, so that we obtain as the final result a de-magnified line image at O of a line source at N or vice versa a magnified line image at N of a line source at O. We infer from Fig. 1 that the ray pattern is symmetric with respect to rotations about an axis through M, which is perpendicular to the drawing plane. In fact, the green, blue, and red ray patterns can be made congruent by appropriate rotations about this axis. The magnification, M_H, in the drawing plane, is therefore given by the ratio $\overline{MN}/\overline{MO}$. Furthermore, we find by an inspection of Fig. 1 and the triangles PC1N and PC2O that $\overline{MN} = \overline{PN} + \overline{MP} = R_1 \sin(\theta_1) \tan(2\theta_1) + R_1 \cos(\theta_1)$ and $\overline{MO} = \overline{PO} - \overline{MP} = R_2 \sin(\theta_2) \tan(180^\circ - 2\theta_2) - R_2 \cos(\theta_2)$ so that

$$\overline{MN} = R_1 \cos(\theta_1) / \cos(2\theta_1) \tag{3}$$

and

$$\overline{MO} = -R_2 \cos(\theta_2) / \cos(2\theta_2) \tag{4}$$

and, because of condition (b),

$$M_H = -\cos(2\theta_2) / \cos(2\theta_1). \tag{5}$$

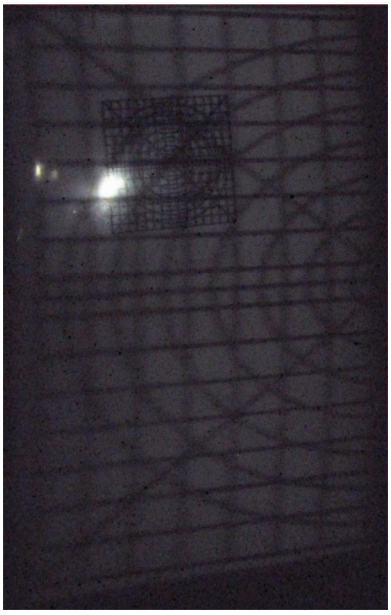

FIG. 2. Image obtained with visible light on a white screen placed at the point N. The insert is a 1:1 copy of the object that was attached to the screen for comparison with the image.

Similarly, the magnification, M_V, perpendicular to the drawing plane, can be derived by considering a rotation of the ray pattern about an axis through M and C2 in the drawing plane, since the ray pattern is symmetric with respect to rotations about any axis through M. The distances of the points N and O from this axis of rotation, are given by $\overline{MN}\sin(\alpha)$ and $\overline{MO}\sin(\alpha)$, where $\alpha = \theta_2$, see dashed lines in Fig. 1, such that

$$M_V = \frac{\overline{MN}\sin(\alpha)}{\overline{MO}\sin(\alpha)} = \frac{\overline{MN}}{\overline{MO}} = M_H \qquad (6)$$

The magnification is therefore uniform and solely a function of the two Bragg angles. It is infinitely large for $\Theta_1 = 45^\circ$.

B. Tests with visible light

The concept of this imaging scheme was tested with visible light, using one convex spherical mirror, with radius $R_1 = 258.4$ mm, and one concave spherical mirror, with radius $R_2 = 609.6$ mm, and Bragg angles of $\Theta_1 = 40^\circ$ and $\Theta_2 = 71^\circ$, respectively. The radius RT of the tangency circle about M was RT = 198 mm, and the theoretically expected magnification was 4.54. For these tests, a transparent foil (target) with orthogonal lines and circles was attached to the surface of a diffuse light panel and placed as an object at the point O in Fig. 1, such that the light panel and target were perpendicular to the drawing plane. In front of the object, at the point P2, was a vertical, 0.2 mm wide, slit. This slit was necessary to reproduce the ray pattern, shown in Fig. 1, with visible light. An image of the target was observed on a white screen, which was positioned at N, see Fig. 1 and a copy of the target was attached to the screen for a direct comparison with the image. The image obtained is shown in Fig. 2.

The overall size of the target was 0.9375 in. × 0.9375 in., the size of the small rectangle was 0.0625 in. × 0.0625 in., and the thickness of the lines was 0.3 mm. Since a 0.2 mm wide slit was used, only a small fraction of the light emitted by the diffuse light panel contributed to the image formation, so that the picture, shown in Fig. 2, was taken with exposure time of $\frac{1}{2}$ h. We infer from Fig. 2 that this imaging scheme produced an undistorted image of a large target of an area of about 1 in. × 1 in. with the theoretically expected uniform magnification of 4.54. Another experiment was performed, using a 60 W filament light bulb as object at O. In this experiment, a bright image of the filament appeared on the screen, such that the structure of the filament and individual turns of the thin filament wires could be resolved with the unaided eye. We point out that a slit is not needed for experiments with x rays, since the ray pattern shown in Fig. 1 will then result from the Bragg condition.

C. Tests with x rays

Tests of the imaging scheme with x rays will be conducted in the near future, using the tungsten Lα–line at 8.3976 keV and a matched pair of spherically bent silicon crystals, a convex Si-422 and a concave Si-533 crystal with 2d-spacings of 2.21707 Å and 1.65635 Å and radii of curvature of 500 ± 1 mm and 823 ± 1 mm, respectively. The crystal surfaces will be parallel to the Bragg reflecting lattice planes to within 10 arcsec. The Bragg angles will be 41.75° and 63.05°. Ray-tracing calculations, which take into account effects of the Johann focusing errors and crystal rocking curves, using Darwin profiles, will be performed for comparison with the experimental data.

ACKNOWLEDGMENTS

This work was supported by DOE by Contract Nos. DE-AC02-09CH-11466 (PPPL) and DE-AC52-07NA-27344 (LLNL).

[1] J. A. Koch, O. L. Landen *et al.*, Appl. Opt.. **37**, 1784 (1998).
[2] R. Tommasini, T. W. Phillips, and J. A. Koch, J. Phys. (France) **133**, 935 (2006).
[3] D. B. Sinars, M. E. Cuneo, G. R. Bennett, and D. F. Wenger *et al.*, Rev. Sci. Instrum. **74**, 2202 (2003).
[4] B. Loupias, F. Perez, A. Bnuzzi-Mounaix, N. Ozaki, M. Rabec, L. E. Glohaec, T. A. Pikuz, A. Ya. Faenov, Y. Aglitskiy, and M. Koenig, Laser Part. Beams **27**, 601 (2009).
[5] G. S. Monk, *Light-Principles and Experiments*, 1st ed. (McGraw-Hill, New York, 1937), p. 52.
[6] M. Dirksmöller, O. Rancu, I. Uschmann, P. Renaudin, C. Chenais-Popovics, J. C. Gauthier, and E. Förster, Opt. Commun. **118**, 379 (1995).
[7] T. Missala, I. Uschmann, E. Förster, G. Jenke, and D. von der Linde, Rev. Sci. Instrum. **79**, 1288 (1999).
[8] S. G. Podorov, A. Nazarkin, and E. Förster, Opt. Commun. **259**, 696 (2006).
[9] M. Bitter, K. W. Hill, S. Scott, R. Feder, Jinseok Ko, A. Ince-Cushman, and J. E. Rice, Rev. Sci. Instrum. **79**, 10E927 (2008).
[10] M. Bitter, K. W. Hill, F. Jones, and S. Scott, J. X-Ray Sci. Technol. **17**, 153 (2009).
[11] M. Bitter, L. F. Delgado, K. W. Hill, S. Scott, R. Ince-Cushman, M. Reinke, Y. Podpaly, J. E. Rice, P. Beiersdorfer, and E. Wang, J. Phys. B **43**, 144011 (2010).
[12] E. Wang, P. Beiersdorfer, M. Gu, M. Bitter, L. Delgado-Aparicio, K. W. Hill, M. Reinke, J. E. Rice, and Y. Podpaly, Rev. Sci. Instrum. **81**, 10E329 (2010).